MODIS Ocean Science Team

Algorithm Theoretical Basis Document

Instantaneous Photosynthetically Available Radiation and Absorbed Radiation by Phytoplankton

(ATBD-MOD-20)

Version 4.0

15 August 1997

Kendall L. Carder, Steve K. Hawes and F. Robert Chen

Marine Science Department
University of South Florida
140 Seventh Avenue South
St. Petersburg, Florida 33701
kcarder@monty.marine.usf.edu

TABLE OF CONTENTS

1.0 Introduction

The algorithm presented here yields three related products, collectively referred to as product MOD21. The first product is the downwelling irradiance just above the sea surface in each of the visible MODIS wavebands, $E_d(\lambda_i,0^+)$, where λ_i = 412, 443, 488, 531, 551, and 667 nm. This portion of the algorithm is based on the maritime irradiance model described in Gregg and Carder (1990).

The second product is instantaneous photosynthetically available radiation, IPAR, which is the total downwelling photon flux just below the sea surface, integrated over the wavelength range 400 to 700 nm. It is called "instantaneous" because it is only a measure of PAR in the instant that the sensor views a given pixel and thus does not represent the irradiance averaged over the entire day. Therefore, IPAR cannot be used directly in primary production models that require PAR values (Platt and Sathyendranath, 1988; Platt et al., 1991). However, it may be possible to relate IPAR to daily PAR values. IPAR is most useful in measuring spatial or day-to-day differences in incident irradiance for comparison with fields of solar-stimulated fluorescence (see Dr. Mark Abbott's ATBD-MOD-23).

The third and most important product is the absorbed radiation by phytoplankton, ARP. It is the total number of photon, or quanta, absorbed by phytoplankton in the top attenuation depth measured at 685 nm, z_{685}. It is determined by multiplying the scalar irradiance and the phytoplankton absorption coefficient at each wavelength and integrating the product from 400 to 700 nm and from the surface to z_{685}. z_{685} is the depth at which $E_d(685,z) = E_d(685,0^-)\cdot e^{-1}$. The main use of ARP is in conjunction with the chlorophyll fluorescence algorithm (product MOD19, ATBD-MOD-23). MOD19 will provide the fluorescence line height, FLH. Dividing FLH by ARP gives a value that is proportional to the quantum yield of fluorescence, which is called chlorophyll fluorescence efficiency, CFE, in ATBD-MOD-23. Even though ARP is the number of quanta absorbed by *all* the phytoplankton pigments, not just by chlorophyll, we will adopt the term CFE for consistency.

2.0 Overview and Background Information

2.1 Experimental Objective

Each of the three products has its own experimental objective. $E_d(\lambda_i,0^+)$ is an interim product. IPAR can be used in primary production research. ARP is the most important product as it is needed to convert FLH into a value that represents the CFE of the phytoplankton. Falkowski and Kolber (1994) suggest that CFE is inversely proportional to the quantum yield of photosynthesis. Because once a photon is absorbed by a viable phytoplankton pigment, its energy must go into photosynthesis, fluorescence, or heat. While the use of FLH and CFE in estimating photosynthetic rates is the subject of much debate, the possibility of using satellites to measure primary production is enticing. CFE has also been demonstrated to be related to nutrient- and/or light-limitation (Keifer, 1973a,b; Carder and Steward, 1985).

2.2 Historical Perspective

Starting with Leckner (1978), a series of simple irradiance models have been developed, e.g., those of Justus and Paris (1985), Bird and Riordan (1986), and Green and Chai (1988). All of these models are specific for terrigenous aerosols, which differ greatly in size and optical characteristics from marine aerosols. The total and spectral irradiance computed using these models can be quite different from the irradiance entering the ocean. The irradiance model of Gregg and Carder (1990) uses a mixture of marine and terrigenous aerosols and is well suited for maritime irradiance calculations. The $E_d(\lambda_i,0^+)$ portion of our algorithm is an adaptation of the Gregg and Carder (1990) model that uses data inputs from MODIS and other EOS sensors.

Measuring global primary production is considered an important goal in oceanography. Satellite measurements of CFE may provide a means of improving estimates of global primary production (Abbott's ATBD-MOD-23).

2.3 Instrument Characteristics

The bulk of the algorithm involves computations on known quantities and data products from MODIS or from other ancillary sources. The instrument characteristics important to this algorithm depend on the other algorithms.

3.0 Algorithm Description

The algorithm calculates the three separate quantities sequentially, $E_d(\lambda_i,0^+)$, IPAR, then ARP. Thus, the physics and mathematics sections below will discuss each output product in turn.

3.1 Theoretical Description

3.1.1 Physics of Problem

Attenuation of solar irradiance in the visible and near-UV wavelengths can be attributed to five atmospheric processes: scattering by the gas mixture (Rayleigh scattering), absorption by ozone, absorption by the gas mixture (primarily by oxygen), absorption by water vapor, and scattering and absorption by aerosols. *Direct* irradiance is not scattered but proceeds directly to the surface of the earth after losses by absorption. *Diffuse* irradiance is scattered out of the direct beam but toward the surface. The sum of the direct and diffuse components defines the downwelling surface irradiance.

Downward irradiance at the sea surface is then attenuated by reflection at the air-sea interface. Reflectance of the direct beam depends on the solar zenith angle and the real part of the index of refraction of seawater. Reflectance of the diffuse irradiance is related to the roughness of the sea surface. Reflectance due to foam can be related to the wind speed, and it affects both the direct and the diffuse components.

The number of quanta absorbed by phytoplankton is calculated as the product of the scalar irradiance and the phytoplankton absorption coefficient integrated over the top attenuation depth.

3.1.2 Mathematical Description of Algorithm

The Gregg and Carder (1990) model is an extension and simplification of the Bird and Riordan (1986) model, and the description here follows their development. The first step in the algorithm is to compute the downwelling irradiance just above the sea surface, $E_d(\lambda,0^+)$, at 1 nm resolution. This spectrum is then binned and weighted appropriately to give the irradiance in each of the visible MODIS channels, $E_d(\lambda_i,0^+)$. Next, the below-surface values are computed, $E_d(\lambda_i,0^-)$, and summed with appropriate weights to give IPAR. Last, scalar irradiance, $E_0(\lambda_i,0^-)$ is multiplied by the phytoplankton absorption coefficient, $a_\varphi(\lambda_i)$, summed with appropriate weighting factors, and integrated over the top attenuation depth to yield ARP.

3.1.2.1 Calculation of $E_d(\lambda_i,0^+)$

$E_d(\lambda,0^+)$ is separated into its direct and diffuse components,

$$E_d(\lambda,0^+) = E_{dd}(\lambda,0^+) + E_{ds}(\lambda,0^+)$$

where the subscripts *dd* and *ds* refer to direct and diffuse components, respectively.

3.1.2.1.1 Direct irradiance – $E_{dd}(\lambda,0^+)$

$E_{dd}(\lambda,0^+)$ is computed by

$$E_{dd}(\lambda,0^+) = F_0(\lambda)\cos(\theta)T_r(\lambda)T_{oz}(\lambda)T_o(\lambda)T_w(\lambda)T_a(\lambda)$$

where $F_0(\lambda)$ is the mean extraterrestrial irradiance corrected for earth-sun distance and orbital eccentricity, θ is solar zenith angle, and T is the transmittance after absorption and/or scattering by each atmospheric component. The components *r, oz, o, w,* and *a* represent Rayleigh scattering, ozone, other gases, water vapor, and aerosols, respectively.

Extraterrestrial solar irradiance — The mean extraterrestrial solar irradiance, $H_0(\lambda)$, is taken from the revised Neckel and Labs (1984) data for the wavelength range of 330 to 700 nm. The extraterrestrial solar irradiance corrected for earth-sun distance is given by Gordon et al. (1983) as

$$F_0(\lambda) = H_0(\lambda)\left\{1 + ecc \cdot \cos\left[\frac{2\pi(JD-3)}{365}\right]\right\}^2$$

where *ecc* is the orbital eccentricity (= –0.0167) and *JD* is Julian day of the year.

Atmospheric path length — The slant path length through the atmosphere, $M(\theta)$, is required for atmospheric transmittance due to attenuation by all constituents. It may be expressed as $1/\cos\theta$ for solar zenith angles < 75°, but a correction for the sphericity of the earth-atmosphere system is required at larger zenith angles. Gregg and Carder (1990) used the empirical formulation of Kasten (1966), but we use an updated formulation from Kasten and Young (1989), which is valid at all zenith angles:

$$M(\theta) = \frac{1}{\cos\theta - 0.50572(96.07995 - \theta)^{-1.6364}}$$

Ozone requires a slightly longer path length for accurate transmittance computations because its dominant concentrations are located in the stratosphere (Paltridge and Platt, 1976):

$$M_{oz}(\theta) = \frac{1.0035}{(\cos^2\theta + 0.007)^{1/2}}.$$

Rayleigh scattering — The Rayleigh total scattering coefficient is taken from Bird and Riordan (1986):

$$T_r(\lambda) = \exp\left[-\frac{M'(\theta)}{(115.6406\,\lambda^4 - 1.335\,\lambda^2)}\right]$$

where λ is in µm and *M'(θ)* is the atmospheric path length corrected for atmospheric pressure,

$$M'(\theta) = M(\theta)\,\frac{P}{P_0}$$

P is the atmospheric pressure and P_0 is standard atmospheric pressure. The normalized water-leaving radiance (L_{wn}) algorithm also requires *P* and will get it from numerical weather models, probably from NMC, according to Dr. Howard Gordon's ATBD-MOD-18. We will take *P* from the same source.

Ozone absorption — Ozone transmittance is computed via

$$T_{oz}(\lambda) = \exp[-a_{oz}(\lambda)\,H_{oz}\,M_{oz}(\theta)]$$

where $a_{oz}(\lambda)$ is the ozone absorption coefficient and H_{oz} is the ozone scale height. Spectral values of $a_{oz}(\lambda)$ are taken from Inn and Tanaka (1953) and differ slightly from those tabulated by Bird and Riordan (1986) due to the higher spectral resolution here. H_{oz} should be available as a MODIS product. If not otherwise known, the ozone scale heights can be estimated from the empirical climatological expression of van Heuklon (1979).

Gas and water vapor absorption — Oxygen is the only atmospheric gas that absorbs significantly in this spectral range. We adopt expressions for transmittance due to oxygen and water vapor absorption from Bird and Riordan (1986):

$$T_o(\lambda) = \exp\left\{-\frac{1.41\,a_o(\lambda)\,M'(\theta)}{\left[1 + 118.3\,a_o(\lambda)\,M'(\theta)\right]^{0.45}}\right\}$$

$$T_w(\lambda) = \exp\left\{-\frac{0.238\, a_w(\lambda)\, WV\, M(\theta)}{[1 + 20.07\, a_w(\lambda)\, WV\, M(\theta)]^{0.45}}\right\}$$

The oxygen and water vapor absorption coefficients (a_o and a_w, respectively) are derived from transmittance calculations with the 5S Code from Tanre et al. (1990), using the high spectral resolution transmittance observations of Kurucz et al. (1984) to obtain 1-nm resolution. *WV* is the total precipitable water vapor in cm, which is MODIS product MOD05. Note that the expression for oxygen gas transmittance uses the pressure-corrected path length, $M'(\theta)$.

Aerosol scattering and absorption — Aerosol concentrations and types vary widely over time and space. Consequently, accurate prediction of their optical thicknesses is difficult. The original Gregg and Carder (1990) model estimated aerosol optical thickness, $\tau_a(\lambda)$, using the Navy aerosol model (Gathman, 1983), which is parameterized by the local meteorological variables "air-mass type", 24 hr. average wind speed, instantaneous wind speed, and relative humidity. Here, life is simpler because the atmospheric correction procedure for MODIS radiances provides the information necessary to compute $\tau_a(\lambda)$.

First, we write the Angstrom formulation for aerosol optical thickness:

$$\tau_a(\lambda) = \beta\, \lambda^{-\alpha} \tag{1}$$

(Van de Hulst, 1981) where β is the turbidity coefficient, which is independent of wavelength and represents the aerosol concentration, λ is wavelength in μm, and α is the Angstrom exponent. We then make a ratio of Eq. 1 at λ = 412 and 667 nm, take the logarithm, and isolate α on the left to get

$$\alpha = \frac{\ln\left[\dfrac{\tau_a(412)}{\tau_a(667)}\right]}{\ln\left[\dfrac{667}{412}\right]}$$

Among the atmospheric correction parameters provided in MODIS product MOD37 are $\tau_a(869)$ and the "epsilon" values, $\varepsilon(\lambda_i,\lambda_j)$, which are defined as:

$$\varepsilon(\lambda_i,\lambda_j) = \frac{\omega_a(\lambda_i)\tau_a(\lambda_i)p_a(\theta,\theta_0,\lambda_i)}{\omega_a(\lambda_j)\tau_a(\lambda_j)p_a(\theta,\theta_0,\lambda_j)}$$

where λ_i and λ_j are any two MODIS wavebands, ω_a is the aerosol single-scattering albedo, and p_a is the aerosol scattering phase function. For marine or non-absorbing aerosols, the approximation

$$\frac{\tau_a(412)}{\tau_a(667)} \approx \frac{\varepsilon(412,869)}{\varepsilon(667,869)} \qquad (2)$$

should be valid (Gordon et al., 1983). Substitution provides our expression to compute α:

$$\alpha = \frac{\ln\left[\dfrac{\varepsilon(412,869)}{\varepsilon(667,869)}\right]}{\ln\left[\dfrac{667}{412}\right]}$$

β is then calculated via

$$\beta = \tau_a(869)\ 869^{\alpha}$$

α and β are then used in Eq. 1 to compute $\tau_a(\lambda)$ and aerosol transmittance is computed by

$$T_a(\lambda) = \exp[-\tau_a(\lambda)\ M(\theta)].$$

The clear-water epsilon product (MOD39, ATBD-MOD-21) flags pixels with highly absorbing aerosols (e.g., Saharan dust). This flag will thus also indicate pixels where the IPAR/ARP products are less accurate, due to the approximation used in Eq. 2.

3.1.2.1.2 Diffuse irradiance – $E_{ds}(\lambda,0^+)$

$E_{ds}(\lambda,0^+)$ is computed via

$$E_{ds}(\lambda,0^+) = I_r(\lambda) + I_a(\lambda) + I_g(\lambda)$$

where I_r, I_a, and I_g represent the diffuse components of incident irradiance arising from Rayleigh scattering, aerosol scattering, and multiple ground-air interactions, respectively. I_g is set to zero because multiple sea surface-boundary-layer/atmosphere interactions are rare (Gordon and Castano, 1987).

Rayleigh scattering — I_r is computed by

$$I_r = F_0 \cos\theta \; T_{oz} T_u T_w T_{aa} (1 - T_r^{0.95}) \cdot 0.5 \tag{3}$$

(λ dependencies are now suppressed) where T_{aa} represents the transmittance after aerosol absorption (not scattering). All of the other components on the right-hand side of the Eq. 3 are computed in the direct irradiance calculations. T_{aa} is given by

$$T_{aa} = \exp[-(1-\omega_a)\tau_a M(\theta)]$$

(Justus and Paris, 1985), where ω_a is the single-scattering albedo of the aerosol. ω_a is computed as

$$\omega_a = (-0.0032\, AM + 0.972)\, e^{0.000306\, RH}$$

where *AM* is the Navy aerosol model air-mass type and *RH* is the percent relative humidity. *AM* ranges from 1 for marine aerosol-dominated conditions to 10 for continental aerosol-dominated conditions. It is assumed to be 1 over the ocean unless the absorbing aerosol flag from MODIS product MOD39 (clear-water epsilon product, ATBD-MOD-21) is set, in which case *AM* is set to 10. We will get *RH* from the same source as does the $[L_w]_N$ algorithm, which will be the output of numerical weather models, probably from NMC, according to ATBD-MOD-18.

Aerosol scattering — I_a is computed by

$$I_a = F_0 \cos\theta \; T_{oz} T_o T_w T_{aa} T_r^{1.5} (1 - T_{as}) F_a$$

where T_{as} represents transmittance due to aerosol scattering only and F_a is the forward scattering probability of the aerosol. T_{as} is computed as

$$T_{as} = \exp[-\omega_a \tau_a M(\theta)]$$

(Justus and Paris, 1985). Following Bird and Riordan (1986), F_a is computed from the following set of equations:

$$F_a = 1 - 0.5 \exp[(B_1 + B_2 \cos\theta) \cos\theta]$$

$$B_1 = B_3[1.459 + B_3(0.1595 + 0.4129\, B_3)]$$

$$B_2 = B_3[0.0783 - B_3(0.3824 + 0.5874\, B_3)]$$

$$B_3 = \ln(1 - \langle\cos\theta\rangle)$$

$\langle\cos\theta\rangle$ is the asymmetry parameter, which is an anisotropy factor for the aerosol scattering phase function as a function of θ (Tanre et al., 1979). In this algorithm, $\langle\cos\theta\rangle$ is given as a function of the aerosol size distribution and can be parameterized in terms of α:

$$\langle\cos\theta\rangle = -0.1417\,\alpha + 0.82$$

For $\alpha < 0.0$, $\langle\cos\theta\rangle$ is set to 0.82, while for $\alpha > 1.2$, $\langle\cos\theta\rangle$ is set to 0.65. This done so that for low α, typical of maritime conditions, the asymmetry parameter converges to the marine aerosol model of Shettle and Fenn (1979), and for high α, typical of continental conditions, the asymmetry parameter converges to that used by Bird and Riordan (1986).

3.1.2.2 Calculation of IPAR

IPAR is defined as

$$IPAR = \frac{1}{hc} \int_{400}^{700} \lambda\, E_d(\lambda, 0^-)\, d\lambda \tag{4}$$

where h is Planck's constant and c is the speed of light. IPAR is calculated from $E_{dd}(\lambda,0^+)$ and $E_{ds}(\lambda,0^+)$ in two steps. First, the sub-surface irradiances are computed. Then the spectra are added together and integrated over the entire spectrum. The downwelling direct and diffuse irradiances just below the sea surface are given by

$$E_{dd}(\lambda, 0^-) = E_{dd}(\lambda, 0^+)(1 - \rho_d)$$
$$E_{ds}(\lambda, 0^-) = E_{ds}(\lambda, 0^+)(1 - \rho_s)$$

where ρ_d is the direct sea surface reflectance and ρ_s is the diffuse sea surface reflectance. Total downwelling irradiance just below the sea surface, $E_d(\lambda,0^-)$ is simply

$$E_d(\lambda, 0^-) = E_{dd}(\lambda, 0^-) + E_{ds}(\lambda, 0^-)$$

3.1.2.2.1 Sea Surface Reflectance

ρ_d and ρ_s are both composed of two terms,

$$\rho_d = \rho_{dsp} + \rho_f$$
$$\rho_s = \rho_{ssp} + \rho_f$$

(Koepke, 1984) where ρ_{dsp} is the direct specular reflectance, ρ_{ssp} is the diffuse specular reflectance, and ρ_f is reflectance due to sea foam. In general, the reflectances are functions of θ and wind speed, but these dependencies have been suppressed for brevity.

ρ_f is a function of sea surface roughness, which in turn has been related to wind speed, *W*

(Koepke, 1984). Using Koepke's (1984) observations, Gregg and Carder (1990) developed the following expressions relating ρ_f to W, which we also use. For $W \leq 4$ m s^{-1},

$$\rho_f = 0$$

for $4 < W \leq 7$ m s^{-1},

$$\rho_f = 0.000022\ \rho_a\, C_D\, W^2 - 0.00040$$
$$C_D = 0.00062 + 0.00156\ W^{-1}$$

and for $W > 7$ m s^{-1},

$$\rho_f = (0.000045\ \rho_a\, C_D - 0.000040)\ W^2$$
$$C_D = 0.00049 + 0.000065\ W$$

where $\rho_a = 1.2 \times 10^3$ g m^{-3} is the density of air and C_D is the drag coefficient. The expressions for C_D are based on those of Trenberth et al. (1989) and on Koepke's observations that $\rho_f = 0$ for $W \leq 4$ m s^{-1}. Comparing ρ_f calculated by the above equations with Koepke's observations yield a root-mean-square (rms) error of 2.54% for the range 4 to 20 m s^{-1}. By not including foam reflectance, the error in total direct reflectance at 20 m s^{-1} for a zenith sun was > 52%. By including this formulation, the error was reduced to 1.2%. Foam reflectance is considered isotropic and thus has no dependence on θ.

ρ_{dsp} is dependent on θ, and for a flat ocean it can be computed directly from Fresnel's law. However, Austin (1974) and Preisendorfer and Mobley (1986) have shown that ρ_{dsp} is also dependent on sea state, which can be related to wind speed. Gregg and Carder (1990) developed the following pair of expressions relating ρ_{dsp} to θ and W, which we also use. First, for $\theta < 40^\circ$ or $W < 2$ m s^{-1},

$$\rho_{dsp}(\theta) = 0.5\left[\frac{\sin^2(\theta-\theta_r)}{\sin^2(\theta+\theta_r)} + \frac{\tan^2(\theta-\theta_r)}{\tan^2(\theta+\theta_r)}\right]$$

where θ is the solar zenith angle and θ_r is the refracted solar zenith angle, which is derived from the expression

$$\frac{\sin\theta}{\sin\theta_r} = n_w$$

where n_w is the index of refraction for seawater, taken to be 1.341 (Austin, 1974). Second, for $\theta \geq 40^o$ and $W \geq 2$ m s^{-1},

$$\rho_{dsp} = 0.0253 \exp[b(\theta - 40)]$$

$$b = -0.000714\, W + 0.0618$$

which is an empirical formulation derived from Austin's data. This empirical expression is only applied where $\theta \geq 40^o$ because Fresnel's law is still approximately valid for all wind speeds up to 2 m s^{-1}. This formulation produced reflectances within 9.5% rms of the data tabulated by Austin, which, incidentally, also agreed with Preisendorfer and Mobley's ray-tracing calculations to within 10% rms, despite Austin's neglect of multiple reflections.

The diffuse specular reflectance ρ_{ssp} is independent of θ. Assuming a smooth sea and uniform sky, it is given a value of 0.066 (Burt, 1954). For a wind-roughened surface (W > 4 m s^{-1}, ρ_{ssp} decreases to 0.057 (Burt, 1954).

3.1.2.2.2 Integration of E_d over wavelength

We approximate the integral in Eq. 4 by using a weighted sum at each of the visible MODIS wavelengths. The new formulation for IPAR is

$$IPAR = \frac{1}{hc} \sum_{i=1}^{6} \lambda_i\, E_d(\lambda_i, 0^-)\, w_{Ed}(i)$$

where λ_i = 412, 443, 488, 531, 551, and 667 nm, and $w_{Ed}(i)$ is the weighting function. The Appendix describes the weighting function and its derivation.

3.1.2.3 Calculation of ARP

The main use of ARP will be as an input to the chlorophyll fluorescence algorithm. Since 90% of the water-leaving radiance is due to scattering in the top attenuation depth (Gordon and McCluney, 1975), we assume that most of the photons fluoresced by chlorophyll which are detected from space also will originate from there. ARP is defined here as

$$ARP = \int_{400}^{700} \int_{0}^{z_{685}} a_{\varphi}(\lambda)\, E_0(\lambda, z)\; dz\, d\lambda \qquad (5)$$

where a_φ is the phytoplankton absorption coefficient, E_0 is the scalar irradiance, and z_{685} is calculated as

$$z_{685} \approx \frac{\cos\theta_r}{a_w(685) + a_{\varphi}(675)} \qquad (6)$$

$a_w(685)$ is the water absorption coefficient at 685 nm, which taken from Smith and Baker (1981), and $a_\varphi(675)$ is taken from the output of the Case 2 chlorophyll algorithm. E_0 is

$$E_0(z) = \frac{E_d(z)}{\bar{\mu}_d(z)} + \frac{E_u(z)}{\bar{\mu}_u(z)} \qquad (7)$$

where E_d and E_u are the downwelling and upwelling irradiances and $\bar{\mu}_d$ and $\bar{\mu}_u$ are the downwelling and upwelling average cosines (the wavelength dependency has been suppressed for brevity). E_d and E_u can be written as

$$E_d(z) = E_d(0^-)\, e^{-K_d z} \quad , \quad E_u(z) = E_u(0^-)\, e^{-K_u z}$$

where z is the depth in m and K_d and K_u are the downwelling and upwelling diffuse attenuation coefficients in m^{-1}, both assumed here to be constant over the depth range of interest. For brevity, lets look at ARP at just any given wavelength, eliminating the wavelength integral in Eq. 5. Substituting Eqs.

6 and 7 into Eq. 5 and taking constant terms outside of the depth integral yields

$$ARP = a_\varphi \frac{E_d(0^-)}{\bar{\mu}_d} \int_0^{z_{685}} e^{-K_d z}\, dz + a_\varphi \frac{E_u(0^-)}{\bar{\mu}_u} \int_0^{z_{685}} e^{-K_u z}\, dz$$

Evaluating the two integrals, we get

$$\int_0^{z_{685}} e^{-K_d z}\, dz = \frac{1 - e^{-K_d z_{685}}}{K_d} \quad , \quad \int_0^{z_{685}} e^{-K_u z}\, dz = \frac{1 - e^{-K_u z_{685}}}{K_u}$$

K_d and K_u can be approximated as

$$K_d \approx (a + b_b)/\bar{\mu}_d \quad , \quad K_u \approx (a + b_b)/\bar{\mu}_u$$

where a is the total absorption coefficient and b_b is the total backscattering coefficient. a is output at the visible MODIS wavelengths by the Case 2 chlorophyll algorithm, and we assume $b_b << a$ and set $b_b = 0$. Then, based on data found in Kirk (1994), $\bar{\mu}_d$ and $\bar{\mu}_u$ are approximated as

$$\bar{\mu}_d \approx 0.96 \cos\theta_r \quad , \quad \bar{\mu}_u \approx 0.4$$

we calculate $E_u(0^-)$ using an expression based on $E_d(0^-)$ and the remote-sensing reflectance, R_{rs}, which is output by the normalized water-leaving radiance algorithm. By the definitions of irradiance reflectance, R, and normalized water-leaving radiance, L_{wn} (Gordon and Clark, 1981), and noting that $L_{wn} = R_{rs} \times F_0$, we have

$$R \equiv \frac{E_u(0^-)}{E_d(0^-)} = L_{wn} \frac{Q\, n_w^2}{F_0[1-\rho(\theta)][1-\rho(\theta_{sat})]}$$
$$= R_{rs} \frac{Q\, n_w^2}{[1-\rho(\theta)][1-\rho(\theta_{sat})]}$$

where Q is the "Q-factor" that relates upwelling irradiance to upwelling radiance, n_w is the seawater refractive index, and θ_{sat} is the satellite viewing angle. Here we set $Q = 4.0$ (Morel and Gentili, 1993) and $n_w = 1.341$, and surface reflectances ρ are computed as in section 3.1.2.2.1. Substituting all of the above equations into Eq. 5 yields the full-blown equation for ARP at any given wavelength. Now we need to integrate that equation over the wavelength range 400 to 700 nm. As in the process for computing IPAR, we use a weighted sum. The full equation is

$$ARP = \sum_{i=1}^{6} a_{\varphi}(\lambda_i) w_{a\varphi}(i) E_d(\lambda_i, 0^-) w_{Ed}(i) \cdot \left[\frac{1 - e^{-K_d(\lambda_i) z_{685}}}{\bar{\mu}_d K_d(\lambda_i)} + \frac{1 - e^{-K_u(\lambda_i) z_{685}}}{\bar{\mu}_u K_u(\lambda_i)} R(\lambda_i) \right]$$

where $w_{a\varphi}$ is the weighting function for phytoplankton absorption. The Appendix describes $w_{a\varphi}$ and how it was determined.

3.1.3 Sensitivity of the Algorithm

We tested the sensitivity of the $E_d(\lambda,0^+)$ portion of the algorithm to variations in $\tau_a(869)$, ozone, water vapor, and aerosol type. We started by generating a baseline $E_d(\lambda,0^+)$ spectrum with $\tau_a(869) = 0.2$, ozone = 275 DU, $WV = 1.5$ cm, and $\alpha = 0.3$. Then we changed the input parameters one-by-one and compared the resulting spectra with to the baseline spectra.

Figure 1 shows a plot of the baseline $E_d(\lambda,0^+)$ spectrum as well as two spectra generated with $\tau_a(869)$ equal to 0.1 and 0.3. Figure 2 shows the ratio of each of the perturbed spectra versus the baseline spectrum. Figure 3 is analogous to Figure 2 except that the perturbed spectra are generated with $\tau_a(869)$ set to the baseline value of 0.2 and ozone values of 300 DU and 250 DU. Figure 4 is like Figures 2 and 3 except that the perturbed spectra have WV equal to 1.25 and 1.75 cm.

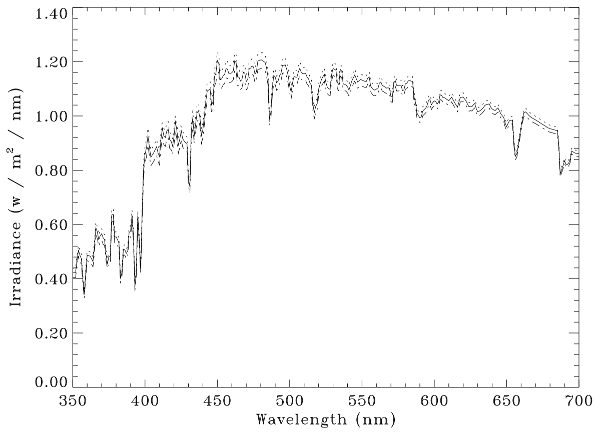

Figure 1. Model calculations of downwelling irradiance above the sea surface, $E_d(\lambda,0^+)$, for W = 12 m/s, $\theta = 47^o$, P = 30.57 inHg, ozone = 275 DU, WV = 1.5 cm, $\alpha = 0.3$, and 3 different values of $\tau_a(869)$: 0.2 (solid line), 0.3 (dashed line), and 0.1 (dotted line).

Effects due to variations in aerosol type were calculated as follows. We chose a marine aerosol with *RH* = 70% and $\alpha(551) = 0.31$ as a candidate model and used its $\varepsilon(\lambda_i,\lambda_j)$ and $\tau_a(869)$ to compute α and $\tau_a(\lambda)$. Then, we varied α by ± 0.1 and plotted the ratios, seen in Figure 5. Figure 6 shows the percentage of the spectral rms errors of the combination of sensitivity tests. The largest effect was for short wavelengths due to uncertainty in $\tau_a(\lambda)$. Spectral errors of less than 5.6% are expected, and errors in IPAR of 5.3% are expected. These percentages are generally equivalent to calibration accuracies of optical sensors deployed in the field.

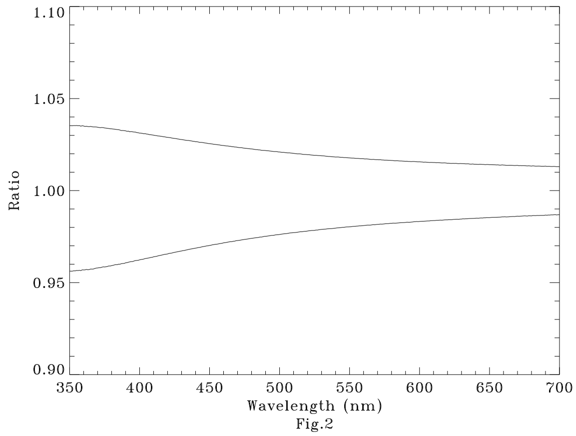

Figure 2. Ratios of $E_d(\lambda,0^+)$ modeled with $\tau_a(869)$ = 0.3 (bottom curve) and $\tau_a(869)$ = 0.1 (top curve) relative to the baseline spectrum.

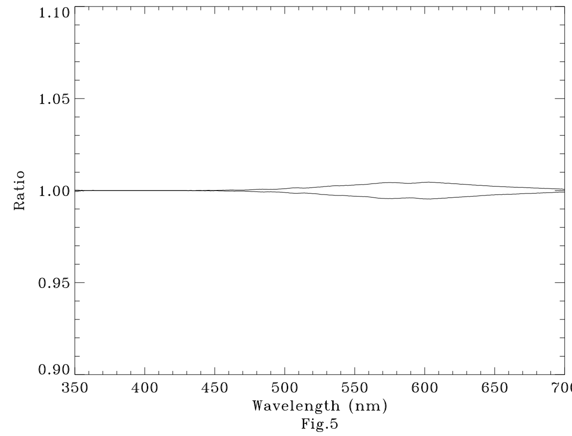

Figure 3. Ratios of $E_d(\lambda,0^+)$ modeled with ozone = 300 DU (bottom curve) and ozone = 250 DU (top curve) relative to the baseline spectrum.

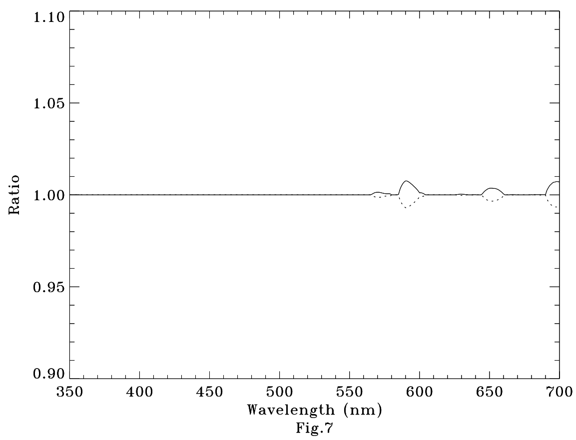

Figure 4. Ratios of $E_d(\lambda,0^+)$ modeled with WV = 1.75 cm (bottom curve) and WV = 1.25 cm (top curve) relative to the baseline spectrum.

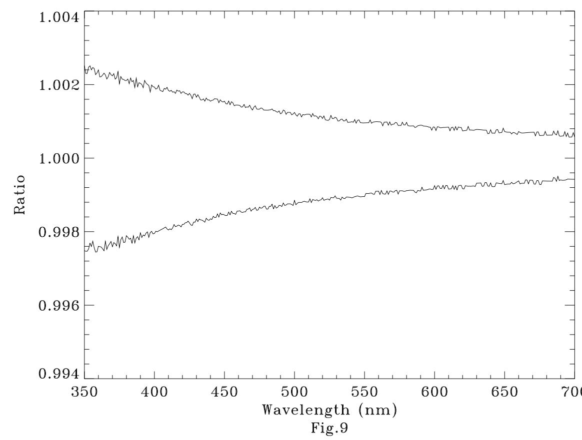

Figure 5. Ratios of $E_d(\lambda,0^+)$ modeled with α = 0.4 (bottom curve) and α = 0.2 (top curve) relative to the baseline spectrum.

For the purpose of measuring $L_{wn}(\lambda)$, a practical upper limit for $\tau_a(869)$ of 0.6 to 1.0 is likely (Gordon and Wang, 1994), limiting conditions under which fluorescence efficiency or remote-sensing reflectance measurements can be obtained. Thus, error analyses for turbid atmospheres are not needed.

3.2 Practical Considerations

It may be possible to output $E_d(\lambda_i,0^+)$ from the MODIS normalized water-leaving radiance algorithm. Since many of the atmospheric computations are similar in both that and in this algorithm, it may save processing time. In that case, the algorithm described here will only be for IPAR and ARP.

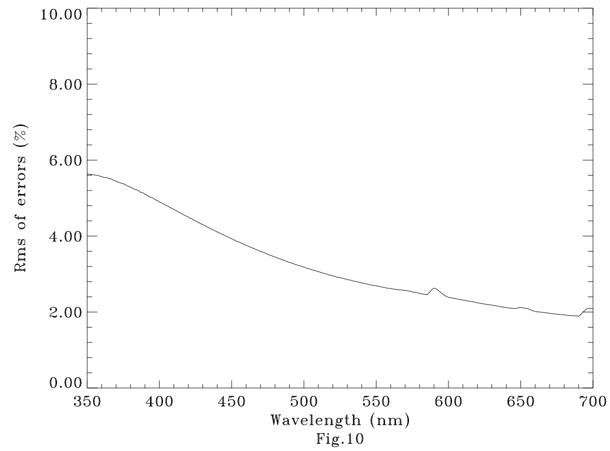

Figure 6. Root-mean-square error spectrum resulting from the sum of all errors (+ and −) depicted in the previous figures.

3.2.1 Numerical Computation

The irradiance model carries a full spectrum from 400 to 700 nm at 1 nm resolution in its computation. If this proves to require too much processing time, the model can be easily pared down to a lower spectral resolution by binning $F_0(\lambda)$ and the atmospheric absorption coefficients accordingly.

3.2.2 Programming/Procedural Considerations

The programming is simple and straight forward. We have followed the procedure outlined in section 3.1.2. The total FORTRAN code is only 600 lines in length.

3.2.3 Calibration and Validation

Gregg and Carder (1990) compared irradiances computed with their model to measurements made with a LiCor LI-1800 spectroradiometer on the ground. For 20,240 individual spectral measurements the model rms error was 6.56% and rms error for PAR was 5.08% for all atmospheric conditions. That is about as accurate as the calibration factor (≈ 5%) of the LiCor.

Since ARP is derived in part from $a_{\varphi}(\lambda)$ which is the largest uncertainty, the accuracy of the estimates of $a_{\varphi}(\lambda_i)$ is expected to be about 30% (see Carder's ATBD-MOD-19).

We will take advantage of the MODIS aerosol network measurements of $E_d(\lambda,0^+)$ and solar transmissivity. We also plan to measure these same variables in the Florida Keys and Fort Jefferson (see ATBD-MOD-21) using AC-9 for in-water absorption measurements. We also will follow Kirk's 1996 method utilizing an integration cavity for total absorption measurements combined with measurements of $a_g(\lambda)$. This will let us avoid the b-factor problem completely. All of these measurements will be used post launch to validate the algorithm. The final product ARP will be combined with Dr. Mark Abbott's MODIS product 23 to provide estimates of fluorescence efficiency (Carder and Steward, 1985). Since fluorescence efficiency varies by over an order of magnitude, our projected accuracy of about 40% for ARP should only weakly contribute to inaccuracies in fluorescence efficiency.

3.2.4 Data Dependencies

Most of the algorithm consists of computations performed on inputs from other MODIS products or other ancillary sources. Table 1 summarizes the data inputs needed for each component of the algorithm.

Table 1. Data inputs needed for each component of the IPAR/ARP algorithm.

$E_d(\lambda_i,0^+)$	$H_0(\lambda)$, θ, JD, P, $a_{oz}(\lambda)$, H_{oz}, $a_o(\lambda)$, $a_w(\lambda)$, WV, $\varepsilon(412,869)$, $\varepsilon(667,869)$, $\tau_a(869)$, AM, RH
IPAR	θ, W
ARP	θ, θ_{sat}, $a_{\varphi}(\lambda_i)$, $a_{\varphi}(675)$, a, $R_{rs}(\lambda_i)$

4.0 Constraints, Limitations, Assumptions

Transmittance of spectral irradiance through the air-sea interface is explicitly accounted for as a function of wind speed, thus incorporating sea surface roughness effects on irradiance reflectance. The surface irradiance is relatively insensitive to 24 hr. mean wind speed, but neglecting variations in current wind speed can produce large errors in estimating light in the water column due to its effect on surface reflectance (Gregg and Carder, 1990). If the current wind speed is not available as a MODIS product, the empirical fit used in the program can avoid these types of gross errors.

If ozone data are not available, the program will use the Van Heuklon model. The model is relatively insensitive to a range in surface air pressure of $P_0 \pm 15$ mb. Therefore, in the absence of observations the standard pressure is sufficient without inducing serious error.

If aerosol optical thicknesses cannot be derived from the other MODIS products (e.g., if this algorithm is to be used for SeaWiFS), then the aerosol optical properties can be derived using the code in the original Gregg and Carder (1990) model. Their approach relied on making a Junge (Junge, 1963) distribution approximation to the Navy aerosol model size distribution. In this case, the entire suite of local meteorological variables are needed. They are air-mass type, 24 hr. average wind speed, instantaneous wind speed, and relative humidity.

Variations in air-mass type can produce significant differences in computed surface irradiance. Determining the air-mass type is not always straightforward but use of the Angstrom exponent from MODIS should provide a reasonably reliable estimate of aerosol type.

The low sensitivity of the model over the evaluated extreme range of relative humidity suggests a reasonable mean value is 80% for use when measurements are not available.

5.0 References

Austin, R. W., The remote sensing of spectral radiance from below the ocean surface. *In* N. G. Jerlov and E. Steemann Nielsen [eds.], *Optical Aspects of Oceanography*, Academic Press, N.Y., pp. 317–344, 1974.

Bird, R. E., and C. Riordan, Simple solar spectral model for direct and diffuse irradiance on horizontal and tilted planes at the earth's surface for cloudless atmospheres, *J. Climatol. Appl. Meteorol.*, 25, 87–97, 1986.

Burt, W. V, Albedo over wind-roughened water, *J. Meteorol.*, 11, 283–289, 1954.

Carder, K. L., and R. G. Steward, A remote-sensing reflectance model of a red-tide dinoflagellate off west Florida, *Limnol. Oceanogr.*, 30, 286–298, 1985.

Falkowski, P., and Z. Kolber, Variations in quantum yield of photosynthesis in marine phytoplankton as measured by active fluorescence, *EOS Trans. AGU*, 75, 232, 1994.

Gathman, S. G., Optical properties of the marine aerosol as predicted by the Navy aerosol model, *Opt. Eng.*, 22, 57–62, 1983.

Gordon, H. R., and D. J. Castano, Coastal Zone Color Scanner atmospheric correction algorithm: Multiple scattering effects, *Appl. Opt.*, 26, 2111–2112, 1987.

Gordon, H. R. and D. K. Clark, Clear water radiances for atmospheric correction of coastal zone color scanner imagery, *Appl. Opt.*, 20, 417–4180, 1981.

Gordon, H. R. and W. R. McCluney, Estimation of the depth of sunlight penetration in the sea for remote sensing, *Appl. Opt.*, 14, 413–416, 1975.

Gordon, H. R., D. K. Clark, J. W. Brown, O. B. Brown, R. H. Evans, and W. W. Broenkow, Phytoplankton pigment concentrations in the Middle Atlantic Bight: Comparison of ship determinations and CZCS estimates, *Appl. Opt.*, 22, 20–36, 1983.

Gordon, H. R., and M. Wang, Retrieval of water-leaving radiance and aerosol optical thickness over the oceans with SeaWiFS: a preliminary approach, *Appl. Opt.*, 33(3), 473–483, 1994.

Green, A. E. S. and S.-T. Chai, Solar spectral irradiance in the visible and infrared regions, *Photochem. Photobiol.*, 48, 477–486, 1988.

Gregg, W. W., and K. L. Carder, A simple spectral solar irradiance model for cloudless maritime atmospheres, *Limnol. Oceanogr.*, 35(8), 1657–1675, 1990.

Inn, E. C. Y. and Y. Tanaka, Absorption coefficient of ozone in the ultraviolet and visible regions, *J. Opt. Soc. Am.*, 43, 870–873, 1953.

Junge, C. E., Air chemistry and radioactivity, Academic, 1963

Justus, C. G. and M. V. Paris, A model for solar spectral irradiance at the bottom and top of a cloudless atmosphere, *J. Climat. Appl. Meteorol.*, 24, 193–205, 1985.

Kasten, F., A new table and approximate formula for relative optical air mass, *Arch. Meteorol. Geophys. Bioklimatol.*, B14, 206–223, 1966.

Keifer, D. A., Fluorescence properties of natural phytoplankton populations, *Mar. Biol.*, 22, 263–269, 1973a.

Keifer, D. A., Chlorophyll a fluorescence in marine centric diatoms: response of chloroplasts to light and nutrients, *Mar. Biol.*, 23, 39–45, 1973b.

Kirk, J. T. O., Light and photosynthesis in aquatic ecosystems, Cambridge Univ. Press, 1994.

Koepke, P., Effective reflectance of oceanic whitecaps, *Appl. Opt.*, 23, 1816–1864, 1984.

Kurucz, R. L., I. Furenlid, J. Brault, and L. Testerman, Solar flux from 296 to 1330 nm, Natl. Solar Obs. Atlas, 1984.

Leckner, B., The spectral distribution of solar radiation at the earth's surface — elements of a model, *Solar Energy*, 20, 143–150, 1978.

Morel, A. Y., and B. Gentili, Diffuse reflectance of oceanic waters (2): bi-directional aspects, *Appl. Opt.*, 32(33), 6864–6879, 1993.

Neckel, H., and D. Labs, The solar radiation between 3300 and 12500 A, *Solar Phys.*, 90, 205–258, 1984.

Paltridge, G. W. and C. M. R Platt, Radiative processes in meteorology and climatology, Elsevier, 1976.

Platt, T., and S. Sathyandranath, Oceanic primary production. Estimation by remote sensing at local and regional scales, *Science*, 241, 285–296, 1988.

Platt, T., C. Caverhill, and S. Sathyandranath, Basin-scale estimates of oceanic primary production by remote sensing: the north Atlantic, *J. Geophys. Res.*, 96, 15,147–15,160, 1991.

Preisendorfer, R. W., and C. D. Mobley, Albedos and glitter patterns of a wind-roughened sea surface, *J. Phys. Oceanogr.* , 16, 1293–1316, 1986.

Shettle, E. P. and R. W. Fenn, Models for the aerosols of the lower atmosphere and the effects of humidity variations on their optical properties, *Air Force Geophys. Lab. Tech. Rep.*, AFGRL-TR-79-0214, 1979.

Smith, R. C., and K. S. Baker, Optical properties of the clearest natural waters (200–800 nm), *Appl. Opt.*, 20, 177–184, 1981.

Tanre, D., M. Herman, P. Y. Deschamps, and A. de Leffe, Atmospheric modeling for space measurements of ground reflectances, including bidirectional properties, *Appl. Opt.*, 18, 3587–3594, 1979.

Tanre, D., C. Deroo, P. Duhut, M. Herman, and J. J. Morcrette, Description of a computer code to simulate the satellite signal in the solar spectrum. The 5S code, *Int. J. Remote Sensing*, 11, 659–668, 1990.

Trenberth, K. E., W. G. Large, and J. G. Olsen, The effective drag coefficient for evaluating wind stress over the oceans, *J. Climatol.*, 2, 1507–1516, 1989.

van Heuklon, T. K., Estimating atmospheric ozone for solar radiation models, *Solar Energy*, 22, 63–68, 1979.

Van de Hulst, H. C., Light Scattering by Small Particles, Dover, N.Y, 1981.

6.0 Appendix — weighting functions for IPAR and ARP calculations

IPAR and ARP are both defined as integrals over the wavelength range from 400 to 700 nm. Since the computations are actually done on spectra of discrete quantities, the integrals are calculated by summing the elements. The $E_d(\lambda_i,0^+)$ portion of the algorithm is designed to provide output in 1 nm intervals — yielding a 301-element spectrum — before binning into the 6 elements representing the visible MODIS wavebands. Thus, the integrals *can* be estimated by summing the 301-element spectrum, but using a weighted sum over the 6-element MODIS spectrum would save processing time. In addition, it is possible that the atmospheric correction code can provide $E_d(\lambda_i,0^+)$, in which case the $E_d(\lambda_i,0^+)$ portion of the IPAR algorithm will not even be used, which in turn will require that a weighted sum be used to estimate the integral. Here we develop weighting factors for both the IPAR and ARP calculations and test them against calculations made on full 301-element spectra.

To develop the weighting functions, we first generate test spectra of $E_d(\lambda,0^-)$ and $a_\varphi(\lambda)$. The $E_d(\lambda,0^-)$ spectrum was generated using RADTRAN (Gregg and Carder, 1990) with the input parameters JD = 100, $\theta = 41^0$, P = 29.92 inHg, AM = 1, RH = 80, WV = 1.5 cm, W = 6 m s^{-1}, ozone = 333 DU, and visibility = 15 km. The $a_\varphi(\lambda)$ spectrum was generated by averaging 48 $a_\varphi(\lambda)$ spectra measured during the TN048 cruise to the Arabian Sea in June and July of 1995. Both spectra are from 400 to 700 nm in 1 nm intervals. The shape of the $a_\varphi(\lambda)$ spectrum is used to choose appropriate wavelength ranges for the six wavelength bins, which are listed in Table 1. The spectra and the bin ranges are depicted in Figure 1.

Table 1. Weighting functions for IPAR and ARP calculations.

λ_i	bin range	w_{Ed}	$w_{a\varphi}$
412	400–427	26.7	1.010
443	428–465	37.4	0.971
488	466–509	45.9	0.985
531	510–541	30.3	1.128

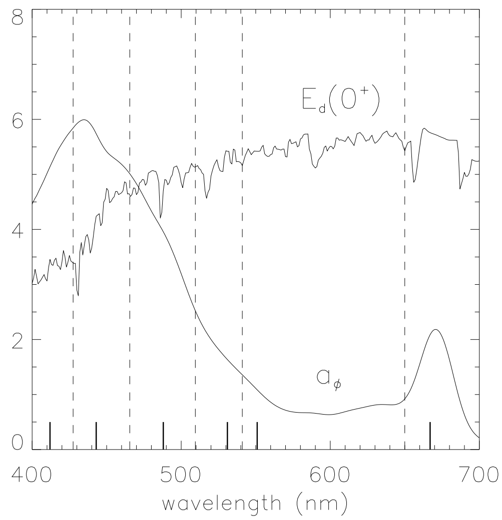

Figure 1. $E_d(\lambda,0^+)$ and $a_\phi(\lambda)$ test spectra used to develop the weighting functions for IPAR and ARP calculations. The vertical dotted lines represent the wavelength bins for the weighting functions. The short, dark vertical lines at the bottom of the chart indicate where λ_i lie. The ordinate is scaled arbitrarily.

551	542–650	111.3	0.732
667	651–700	47.2	0.601

The IPAR weighting function, $w_{Ed}(i)$, is determined via

$$w_{Ed}(i) = \frac{\int_{\Delta\lambda_i} E_d(\lambda, 0^-)\, d\lambda}{E_d(\lambda_i, 0^-)}$$

where $\Delta\lambda_i$ is the wavelength range for the bin corresponding to λ_i. Likewise, the ARP weighting function, $w_{a\varphi}(i)$, is determined via

$$w_{a\varphi}(i) = \frac{\int_{\Delta\lambda_i} a_\varphi(\lambda)\, d\lambda}{a_\varphi(\lambda_i)\int_{\Delta\lambda_i} d\lambda}$$

The integrals are approximated by sums over the 1 nm-increment spectra. The values of $w_{Ed}(i)$ and $w_{a\varphi}(i)$ are listed in Table 1.

The accuracy of using the weighting functions to calculate IPAR was tested using 14 different $E_d(\lambda,0^-)$ spectra. These were generated by RADTRAN using permutations of four varying input parameters. This creates 16 (i.e., 2^4) possible spectra, but two were not used because the combination of input parameters is unrealistic. The four input parameters and the 2 possible values they can be given are $\theta = (10^\circ,60^\circ)$, visibility = (5 km,50 km), AM = (1,10), and W = (1 m s^{-1}, 30 m s^{-1}). IPAR was calculated both as the sum of $E_d(\lambda,0^-)$ over all wavelengths (RADTRAN output is in 1 nm intervals) and as the weighted sum and the results for each spectrum were compared. The mean ± standard deviation of the ratio of the IPAR values (full sum:weighted sum) was 1.0033 ± 0.0042 and the range was from 0.9997 to 1.0148. Thus, for the $E_d(\lambda,0^-)$ spectra tested here, the biggest error was about 1.5%, which was for $\theta = 60^\circ$, visibility = 5 km, AM = 10, and W = 1 m s^{-1}.

The accuracy of using the ARP $E_d(\lambda,0^-)$ weighting function was tested using the same 14 spectra and the same $a_\varphi(\lambda)$ spectrum as above. For the purposes of this test, ARP was approximated as $E_d(\lambda,0^-)$ x $a_\varphi(\lambda)$. ARP was calculated both as the sum over all wavelengths and as the weighted sum and the results for each spectrum were compared. The mean ± standard deviation of the ratio of the ARP values (full sum:weighted sum) was 1.0011 ± 0.0018 and the range was from 0.9995 to 1.0058.